JAST, Vol. 3, No. 2, pp 67–75

JAST
Journal of Aerospace Science and Technology

Numerical Simulation of Scaling Effect on Bubble Dynamics in a Turbulent Flow around a Hydrofoil

M. Mahdi[1], M. Shams[2], R. Ebrahimi[3]

A Lagrangian-Eulerian numerical scheme for the investigation of bubble motion in turbulent flow is developed. The flow is analyzed in the Eulerian reference frame while the bubble motion is simulated in the Lagrangian one. Finite volume scheme is used, and SIMPLEC algorithm is utilized for the pressure and velocity linkage. The Reynolds stresses are modeled by the RSTM model of Launder. Upwind scheme is used to model convective fluxes. The Guassian Filter White Noise is incorporated to simulate the turbulent fluctuation velocities. The bubble diameter is found by the use of Rayleigh-Plesset equation. Various forces in the equation of motion of the bubble are considered. The Buoyancy, Saffman lift, drag, pressure, and change of volume forces are carefully applied. The effects of all of these forces on bubble path are also examined. The bubbles are created in the low pressure zones, and then traced in the flow field. It is observed that the bubble diameter is highly dependent on the mean stream pressure, and its location. The results are compared with the other published works, and have an acceptable accuracy.

INTRODUCTION

In the liquid flow, cavitation generally occurs if the pressure in certain locations drops below the vapor pressure and consequently the negative pressure is relieved by the formation of gas-filled or gas and vapor-filled cavities. Cavitation occurs by the sudden expansion and the volumetric oscillation of bubble nuclei in the water due to the ambient pressure change. The size of bubble nuclei is in the order of O(10 μm) [1]. Formation and collapse of bubble in liquids are used in many technical applications such as lithotripsy,ultrasonic cleaning, bubble chambers, and laser surgery [2]. Bubbledynamics has been the subject of intensive theoretical and experimental studies since Lord Raleigh (1917) found the well-known analytic solution to this problem for inviscid liquids. The advanced theory of cavitation was developed by Plesset (1949), who found the differential Rayleigh – Plesset (RP) equation for the bubble radius [3]. The RP equation described the dynamics of a spherical void or gas bubble in viscous liquids, and is also used as a first approximation in more complex problems such as cavitation near solid boundaries. Cavitation could be observed in a wide variety of propulsion and power systems like pumps, nozzles, injection, marine propellers, hydrofoils and underwater bodies.

Two-phase flow could be analyzed as two fluids in the Eulerian/Eulerian approach, or as a continuum phase and another bubble phase in the Eulerian/Lagrangian or trajectory approach. The bubble equation of motion is solved simultaneously with the RP equation to determine its trajectory (Eulerian/Lagrangian method) [4].

Meyer et al [5] correlated a numerical simulation of the cavitation on a Schiebe headform. They developed a computer code to statistically model cavitation inception, consisting of a numerical solution to the RP equation coupled to a set of trajectory equations. Using the code, trajectories and growths were computed for bubble of varying initial sizes. An off-body distance was specified along the $C_p = 0$, and the bubble was free to follow an off-body trajectory. They also showed that the cavitation inception is sensitive to nuclei distribution.

1. *PhD Candidate, Dept. of Mech. Eng., K.N. Toosi Univ. of Tech. Tehran, Iran.*
2. *Associate Professor, Dept. of Mech. Eng., K.N. Toosi Univ. of Tech., Tehran, Iran, E-mail: Mehrzad_shams@yahoo.com.*
3. *Associate Professor, Dept. of Aerospace Eng., K.N. Toosi Univ. of Tech., Tehran, Iran.*

Chahine [6] has pursued a different approach to the study of dynamics of traveling cavitation inception bubbles using inviscid potential flow, but including the modifications of the flow by the nucleus, and allowing the nucleus to deform. These calculations have provided detailed information about the capture, growth, and collapse of a single bubble in a Rankine vortex.

Kevine J. Farrell [7] developed an Eulerian/Lagrangian computational procedure for the prediction of the cavitation inception. The trajectories were computed using Newton's second law with models for various forces acting on the bubble. The growth was modeled using RP equation. Cavitation inception data show that inception indices generally decrease with increasing velocity, which is contrary to expectations based on the increased flux of nuclei to the minimum pressure region.

Can F. Delate and et al. [8] consider quasi-one-dimensional steady-state cavitating nozzle flows by taking into account the effect of bubble nucleation. The nonlinear dynamics of cavitating bubbles is described by the classical RP equation where a polytropic law for the partial gas pressure is employed by taking into account the effect of damping mechanisms by an effective viscosity.

Zhang and Ahmadi [9] recently computed an Eulerian-Lagrangian computational model for simulations of gas-liquid-solid flows in three phase slurry reactors. They used a two-way interaction between bubble-liquid and particle-liquid. but, they did not consider the bubble growth in their analysis.

In this research, the bubble dynamics in turbulent flow around a 2-d hydrofoil of NACA0015 is analyzed. The chord length is 115mm. A finite volume code is used to analyze the flow field and the results were verified by the experimental data. A numerical code for bubble motion is developed. An equation is written for bubble motion in Lagrangian reference frame. Saffman lift force that is ignored in the previous researches, is considered, and compared with the other forces in bubble line movement. The growth was modeled using the RP equation. The effects of any slip velocity between the bubble and the carrying liquid are also considered. GFWN model is used to simulate turbulent velocity fluctuations. Also, the effect of parameters such as fluctuating velocity components, cavitation number, initial radius and the angle of attack on bubble dynamics is also investigated.

FLOW SIMULATION

Since the flow is turbulent it is important to use an appropriate turbulence model for evaluating the mean-flow field. Reynolds stress transport model (RSTM) of Launder et al [10] is used in this study. This model accounts for the evolution of individual turbulence stress components, and is well suited for handling anisotropic turbulence stress.

Mean-flow model

For an incompressible fluid flow, the equation of continuity and balance of momentum for the mean motion are given as:

$$\frac{\partial \bar{u}_i}{\partial x_i} = 0,$$

$$\frac{\partial \bar{u}_i}{\partial t} + \bar{u}_j \frac{\partial \bar{u}_i}{\partial x_j} = -\frac{1}{\rho}\frac{\partial \bar{p}}{\partial x_i} + \upsilon \frac{\partial^2 \bar{u}_i}{\partial x_j \partial x_j} - \frac{\partial}{\partial x_j} R_{ij}, \qquad (1)$$

Where $\bar{u}_i$ is the mean velocity, x_i is the position, t is the time, $\bar{P}$ is the mean pressure, ρ is the constant mass density, υ is the kinematics viscosity, and $R_{ij} = \overline{u'_i u'_j}$ is the Reynolds stress tensor. Here, $u'_i = u_i - \bar{u}_i$ is the fluid fluctuation velocity component.

The RSTM accounts for differential transport equations for evaluation of the turbulence stress components. i.e.

$$\frac{\partial}{\partial t} R_{ij} + \bar{u}_k \frac{\partial}{\partial x_k} R_{ij} = \frac{\partial}{\partial x_k}\left(\frac{\upsilon_t}{\sigma^k}\frac{\partial}{\partial x_k} R_{ij}\right) - \left[R_{jk}\frac{\partial \bar{u}_j}{\partial x_k} + R_{jk}\frac{\partial \bar{u}_i}{\partial x_k}\right] - C_1 \frac{\epsilon}{k}\left[R_{ij} - \frac{2}{3}\delta_{ij} k\right] - C_2\left[P_{ij} - \frac{2}{3}\delta_{ij} P\right] - \frac{2}{3}\delta_{ij}\epsilon, \qquad (2)$$

where the turbulence production terms are defined as:

$$P_{ij} = -R_{jk}\frac{\partial \bar{u}_j}{\partial x_k} - R_{jk}\frac{\partial \bar{u}_i}{\partial x_k},$$

$$P = \frac{1}{2} P_{ij}. \qquad (3)$$

With P being the fluctuation kinetic energy production. Here ν_t is the turbulent (eddy) viscosity; and $\sigma^k = 1.0, C_1 = 1.8, C_2 = 0.6$ are empirical constants. The turbulence dissipation rate, ϵ, is computed by the governing equation:

$$\frac{\partial \epsilon}{\partial t} + \bar{u}_j \frac{\partial \epsilon}{\partial x_i} = \frac{\partial}{\partial x_i}\left[\left(\upsilon + \frac{\upsilon_t}{\sigma^\epsilon}\right)\frac{\partial \epsilon}{\partial x_j}\right] - C^{\epsilon 1}\frac{\epsilon}{k} R_{ij}\frac{\partial \bar{u}_i}{\partial x_j} - C^{\epsilon 2}\frac{\epsilon^2}{k}. \qquad (4)$$

In Eq.(2,4), $k = \frac{1}{2}\overline{u'_i u'_i}$ is the fluctuation kinetic energy, and ϵ is the turbulence dissipation. The values of constants are [11]:

$$\sigma^\epsilon = 1.3, C^{\epsilon 1} = 1.44, C^{\epsilon 2} = 1.92. \qquad (5)$$

Fluctuating velocity

Dispersion of small particles is strongly affected by the instantaneous fluctuation fluid velocity. The turbulence fluctuations are random functions of space and time. In this study, the continuous filter white-noise (CFWN) model described by Thomson [12] is used to generate instantaneous fluctuating fluid velocity. Accordingly, the ith component of instantaneous fluid velocity satisfies the following stochastic equation [13]:

$$\frac{du_i}{dt} = -\frac{u_i - \bar{u}_i}{T_I} + \left(\frac{2\bar{u'}_i^2}{T_I}\right)^{\frac{1}{2}} \zeta_i(t), \tag{6}$$

Here, $\bar{u'}_i^2$ is the mean-square of the ith fluctuation velocity, and the summation convention on the underlined indices is suspended. In equation (6), T_I is the particle integral time, which is the average time spent in turbulent eddies along the particle path,

$$T_I = \int_0^\infty \frac{\overline{u'_p(t)u'_p(t+s)}}{u'_q u'_q} ds, \tag{7}$$

for small particles that move with the fluid, the particle integral time may be approximated by the fluid point Lagrangian integral time T_1. The latter is related to fluctuating kinetic energy and dissipation rate, i.e.

$$T_L = C_L \frac{k}{\epsilon}, \tag{8}$$

with the constant $C_L \approx 0.3$ (Daly and Harlow [14]). Therefore,

$$T_l \approx T_L \approx 0.3\frac{k}{\epsilon}. \tag{9}$$

In equation (6), $\zeta_i(t)$ is a Gaussian vector white noise random process white spectral intensity S_{ij}^n given by:

$$S_{ij}^n = S_0 \delta_{ij}, \tag{10}$$

where

$$S_0 = \frac{1}{\pi}. \tag{11}$$

In the numerical simulation, the amplitude of $\zeta_i(t)$ at every time step is given as:

$$\zeta_i(t) = \frac{G_i}{\sqrt{\Delta t}}, \tag{12}$$

where G_i is a zero-mean, unit variance independent Gaussian random number and Δt is the time step used in the simulation. Each entire time sample is then shifted randomly between 0 to Δt to generate an appropriate white-noise time history.

The CFWN simulation technique described here has several advantages over other available techniques. It provides correct turbulent intensities and accounts for the proper time scale of turbulence. More importantly, the model leads to the correct magnitude of turbulent diffusivity for fluid point particles. In addition, the model is convenient to apply and is computationally efficient.

IMPROVED SPHERICAL BUBBLE DYNAMICS MODEL

The behavior of spherical bubble in a pressure field is usually described with a relatively simple bubble dynamics model known as the Rayleigh – Plesset equation (Plesset 1948) [15]:

$$R\ddot{R} + \frac{3}{2}\dot{R}^2 = \frac{1}{\rho}\left[p_v + p_g - p - \frac{2\gamma}{R} - \frac{4\mu}{R}\dot{R}\right], \tag{13}$$

where R is the time dependent bubble radius, ρ is the liquid density, p_v is the vapor pressure, p_g is the gas pressure inside the bubble, p is the ambient pressure local to the bubble, μ is the liquid viscosity, γ is the surface tension. If the gas is assumed to be perfect and to follow a polytrophic compression relation, then one has the following relationship between the gas pressure and the bubble radius:

$$p_g = p_{g0}\left(\frac{R_0}{R}\right)^{3k}, \tag{14}$$

where p_{g0} and R_0 are the initial gas pressure and bubble radius respectively and is the polytrophic gas constant. The internal process inside the bubble is assumed to be isentropic. In equation (13) the bubble grows principally in response to a change in the ambient pressure through gaseous expansion, and increase in the vaporous mass within the bubble. A one way analysis is adopted and the effect of the bubble on the liquid is ignored. In addition, equation (13) does not take into account the effect of any slip velocity between the bubble and the carrying liquid. To account for this slip velocity, an additional pressure term $\frac{\rho(\vec{U}-\vec{U}_b)^2}{4}$ is added to the classical Rayleigh – Plesset equation [16,17].

$$R\ddot{R} + \frac{3}{2}\dot{R}^2 = \frac{1}{\rho}\left[p_v + p_g - p - \frac{2\gamma}{R} - \frac{4\mu}{R}\dot{r}\right] + \frac{\rho\left(\vec{U} - \vec{U}_b\right)^2}{4}. \tag{15}$$

Virtually all liquids contain some dissolved gas. Indeed it is virtually impossible to eliminate this gas from any substantial liquid volume. If the nucleation bubble contains some gas, then the pressure in the

bubble is the sum of the partial pressure of this gas, p_G, and the vapor pressure. Hence the equilibrium pressure in the liquid is:

$$p = p_V + p_G - \frac{2\gamma}{R}, \tag{16}$$

where R is the time dependent bubble radius, p_v is the vapor pressure, p_g is the gas pressure inside the bubble, p is the ambient pressure local to the bubble, γ is the surface tension. In the context of cavitation flow, it is appropriate to assume that the microbubble of radius R_0 is in equilibrium at $t = 0$ in the fluid at pressure p so that:

$$p_{G0} = p - p_V(T_\infty) - \frac{2\gamma}{R_0}. \tag{17}$$

The general features of solution RP equation under this initial condition are characteristic of the response of a bubble as it passes through any low-pressure region.

For the purposes of the present discussion, we shall consider a steady, single-phase flow of a Newtonian liquid of constant density, ρ, velocity field, U, and pressure, p. In all such flow it is convenient to define a reference velocity, U_∞ and p_∞ which are conventionally the velocity and pressure of the uniform and upstream flow respectively. The pressure coefficient is defined as:

$$C_p(x,y) = \frac{p(x,y) - p_\infty}{\frac{1}{2}\rho U_\infty^2}. \tag{18}$$

There will be some locations, x_i, y_i, within the flow where $C_p(x_i, y_i)$ and p are minimum, and that value of $C_p(x_i, y_i)$ will be denoted for convenience by $C_{p\min}$. For a given geometry, $C_p(x_i, y_i)$ and $C_{p\min}$ are functions of Reynolds number in the steady flow. When the overall pressure is decreased or the flow velocity is increased, the pressure at some point in the flow approaches the vapor pressure p_V, of the liquid at the reference temperature T_∞. In order to characterize this relationship, it is conventional to define the cavitation number, σ as:

$$\sigma = \frac{p_\infty - p_V}{\frac{1}{2}\rho U_\infty^2}. \tag{19}$$

Any flow, whether cavitating or not, has some value of σ. Clearly if σ is sufficiently large, single phase liquid flow will occur. However, as σ is reduced, nucleation will first occur at some particular value of σ called the incipient cavitation number.

BUBBLE MOTION EQUATION

The motion equation of a spherical particle subjected to the force of gravity in a fluid has been derived by several prominent scientists such as Basset [17], Boussinesq [18] and Maxey [19]. Use of numerical simulation to study particle dispersion and deposition in the turbulent flows was reported by Ahmadi [20] and Shams et al [21]. By considering the forces acting on the spherical bubble with radius R, the equation of motion is:

$$\begin{aligned}\rho_b V_b \frac{d\vec{U}_b}{dt} &= V_b(\rho_b - \rho)g\vec{j} + V_b\vec{\nabla}p \\ &+ \frac{1}{2}\rho A_b C_D(\vec{U} - \vec{U}_b)\left|\vec{U} - \vec{U}\right| \\ &+ \frac{1}{2}\rho V_b\left(\frac{d\vec{U}}{dt} - \frac{d\vec{U}_b}{dt}\right) + \frac{1}{2}\rho\left(\vec{U} - \vec{U}_b\right)\frac{dV_b}{dt} \\ &+ 1.615\rho\upsilon^{\frac{1}{2}}d^2\left(\vec{U} - \vec{U}_b\right) * \left|\frac{d\vec{U}}{dy}\right|^{\frac{1}{2}} Sgn\left(\frac{d\vec{U}}{dy}\right)\vec{j}\end{aligned} \tag{20}$$

where terms with the subscript b are related to the bubble and those without a subscript are related to the carrying fluid. V_b and A_b are the bubble volume and projected area, which are equal to $\frac{4}{3}\pi R^3$ and πR^2 respectively. The bubble drag coefficient C_D in equation (20) can be determined by using the empirical equation of Hagerman and Morton (1953) [22] :

$$\begin{aligned}C_D &= \frac{24}{\mathrm{Re}}\left(1 + 0.197\,\mathrm{Re}^{0.63}\right) + \frac{24}{\mathrm{Re}}\left(2.6\times10^{-4}\,\mathrm{Re}^{1.38}\right), \\ \mathrm{Re} &= \frac{2R|U - U_b|}{\upsilon}.\end{aligned} \tag{21}$$

The physical meaning of each term in the right hand side of equation (20) is as follows. The first term is the buoyancy force. The second term is due to the pressure gradient in the fluid surrounding the particle. The third term is the drag force. The fourth term is the force to accelerate the virtual "added mass" corresponding fluid. The fifth term is the force due to the bubble volume variation, and the last term is the lift force, which is caused by the bubble spin. By dividing the two sides of equation (20) to ρV_b, the final equation is achieved as follows:

$$\begin{aligned}\frac{d\vec{U}_b}{dt} &= 2g\vec{j} - \frac{3}{\rho}\nabla\vec{p} \\ &+ \frac{3}{4}\frac{C_D}{R}\left(\vec{U} - \vec{U}_b\right)\left|\vec{U} - \vec{U}_b\right| + \frac{3}{R}\left(\vec{U} - \vec{U}_b\right)\dot{R} \\ &+ \frac{1.542}{R}\upsilon^{\frac{1}{2}}\left(\vec{U} - \vec{U}_b\right) * \left|\frac{d\vec{U}}{dy}\right|^{\frac{1}{2}} Sgn\left(\frac{d\vec{U}}{dy}\right)\vec{j}\end{aligned} \tag{22}$$

RESULTS

Flow and bubble motion around a 2-D hydrofoil is investigated. A C type grid is generated in the physical

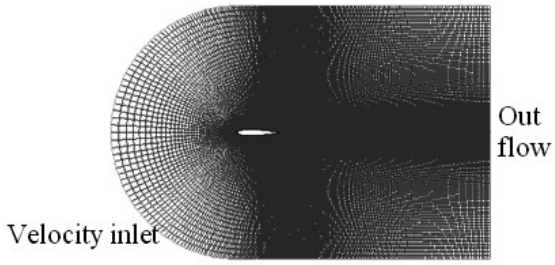

Figure 1. Generated grid in the physical domain

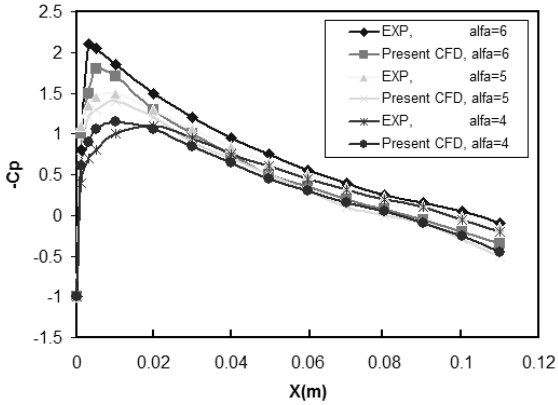

Figure 2. Pressure coefficient for different angle of attacks in the present numerical simulation and experimental data [23] for $\mathrm{Re} = 8 \times 10^5$.

domain and is shown in Figure 1. Grid independency check is also done here, and the optimum number of the computational cells is approximately 48000. "Velocity inlet" type and "fully developed" is used for the boundary conditions. The grid spacing is suitably fined in the near wall regions. The first node adjacent to the wall is located between $50<y^+<500$, in which y^+ is dimensionless distance away from the wall, and $+$ stands for dimensionless turbulent wall units.

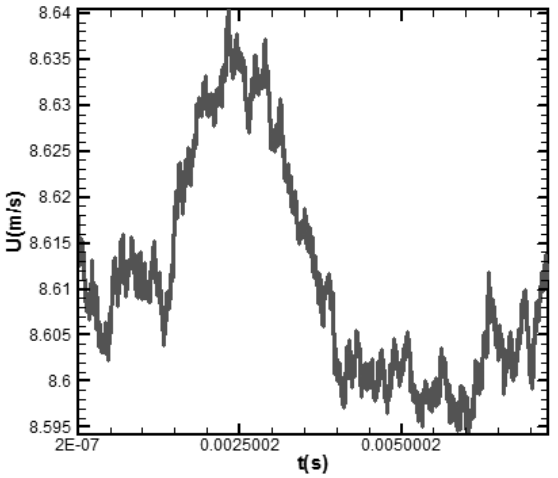

Figure 3. Instantaneous velocity component at one point near the outflow in the flow field.

The variation of C_p in the chord direction for different angle of attacks is illustrated in Figure 2. The flow Reynolds number is $\mathrm{Re} = 8 \times 10^5$. The present results are compared with the cavitation tunnel test data collected by Rapposelli et al [23]. Tremendous pressure variations in the leading edge of the hydrofoil are observed.

The velocity fluctuations have a significant effect on the bubble size and its trajectory. Some of the previous researches ignored this effect. Here, by using the CFWN model velocity components are calculated. Figure 3 shows the instantaneous velocity at one specific point near the outflow in the domain for $\mathrm{Re} = 8 \times 10^5, \alpha = 4^0$.

The corresponding sample trajectory of the bubble with and without fluctuation components are illustrated in Figure 4a. The bubble radius of these two samples is presented in Figure 4b. Fluctuating velocity components intensify the variation of bubble diameter and size. The turbulence intensity directly affects the velocity fluctuations and consequently the bubble size.

Various forces are considered in this simulation, and their effect is presented in Figure 5. The initial condition parameters are $\mathrm{Re} = 8 \times 10^5$ $R_\circ = 50\mu m$ and $\alpha = 4°$. Pressure gradient force in the horizontal and vertical coordinates are shown in Figure 5a, b. It shows that this force is only significant in the low pressure regions at the leading edge of the hydrofoil. Because of the bubble growth at these low pressure regions, the drag force increases and this effect is presented in Figure 5c,d. The simulation shows that the Saffman Lift force is negligible in comparison with other forces and is shown in Figure 5e. The force due to volume change is calculated and presented in the Figure 5f. This force has a significant value especially at the low pressure regions because of its rapid bubble growth.

The effect of the above mentioned forces on the bubble radius and trajectory is also examined and presented in Figure 6. The bubble radius during its motion at cavitation numbers of 0.98, 0.64, 0.57 is shown in Figure 6a. By decreasing the cavitation number, a large bubble diameter is observed, i.e. for $\sigma = 0.57$ a huge bubble growth at the leading edge is seen. The bubble size is oscillatory at low pressure regions because of these mechanisms. While the bubble radius changes, its trajectory is also affected by these forces as shown in Figure 6b. According to this figure, although all bubbles are released for the same point with the same initial size, their trajectories are deviating and scattering because of these forces due to mainly different cavitation numbers. The effect of initial bubble diameter on its trajectory is illustrated in Figure 7. Bubbles are released from the $\mathrm{Re} = 8 \times 10^5, \sigma = 0.98$, and the angle of attack is $\alpha = 4$. The initial radius of 25, 50, 75, and 100 micron is examined here.

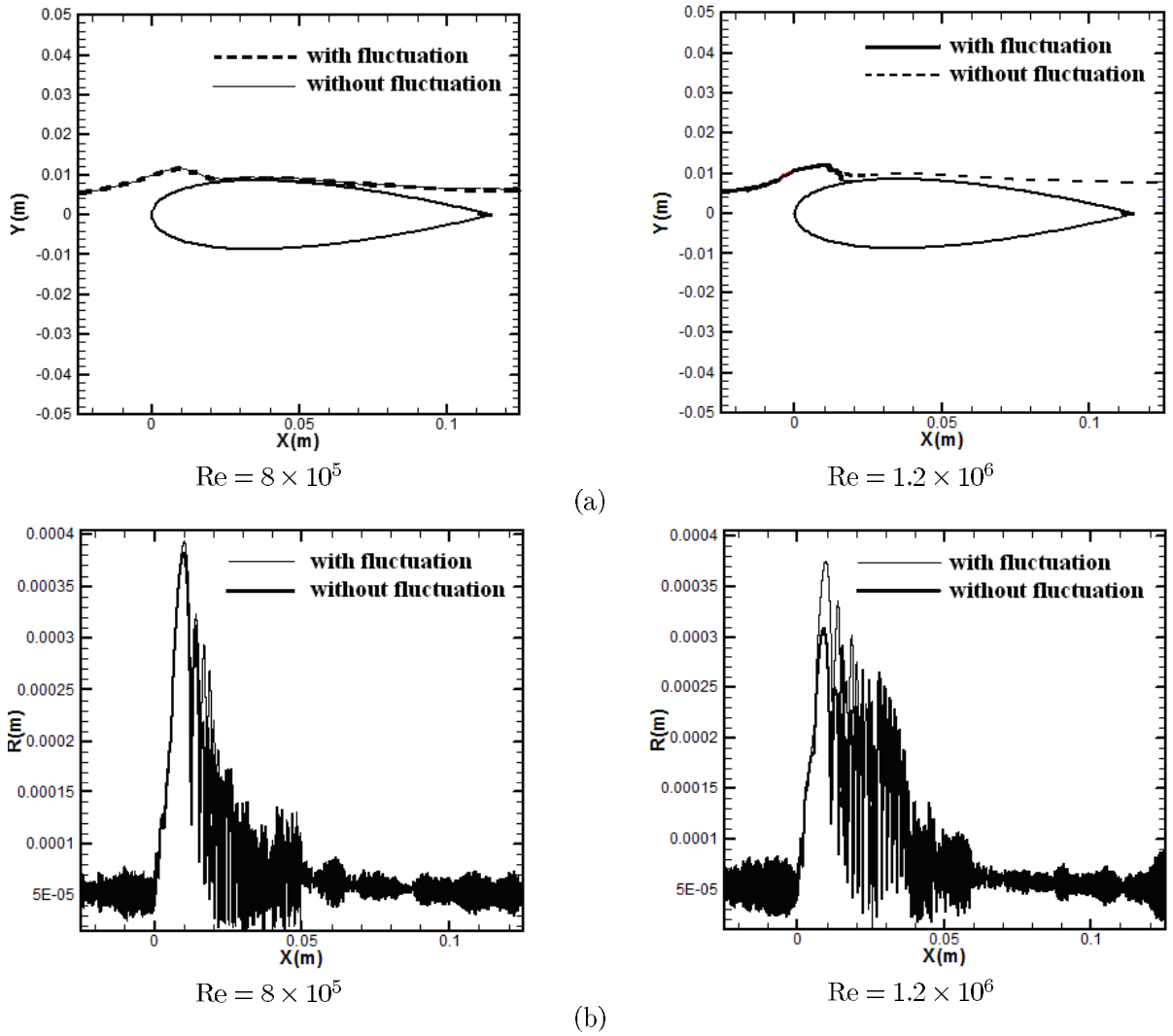

Figure 4. Bubble dynamics at $\alpha = 4°$ for different turbulent intensity: (a) bubble trajectory and (b) bubble radius.

The bubbles are following the same path before touching the low pressure zone. They will deviate from the original path due to sharp variations in the leading edge. The significant force that changes bubble path is the force due to volume change. For this reason, the bubble that has a 100 micron radius is colliding with the wall while the others exit with any collision from the region.

The effect of angle of attack is also checked here. Attack angle also has a significant effect on pressure distribution that is shown in Figure 8a. A zero angle of attack is used. Two bubbles with the same initial diameter are released while the cavitation number is different. The bubbles that have $\sigma = 0.68$ will reach the wall. These parameters are also examined with angle of attack of $\alpha = 6$ and are shown in Figure 9. The fluid flow static pressure is illustrated in Figure 9a. The bubble trajectory is also examined carefully in the leading edge and is presented in Figure 8b. It is observed that the bubble is not touching the hydrofoil wall while it is in the previous figure. The streamlines and pressure distribution are significantly affected by the angle of attack

CONCLUSION

The bubble dynamics is analyzed by using an Eulerian-Lagrangian approach. The effect of various parameters like fluctuating velocity component, cavitation number, angle of attack and the bubble initial radius; on the bubble dynamics is examined. According to the obtained results, the following conclusions are drawn:

- Drag force, saffman lift, pressure gradient and buoyancy forces are effecting the bubble movement. These forces are functions of the bubble position, the bubble diameter and flow parameters. The force due to volume change significantly influences bubble dynamics.

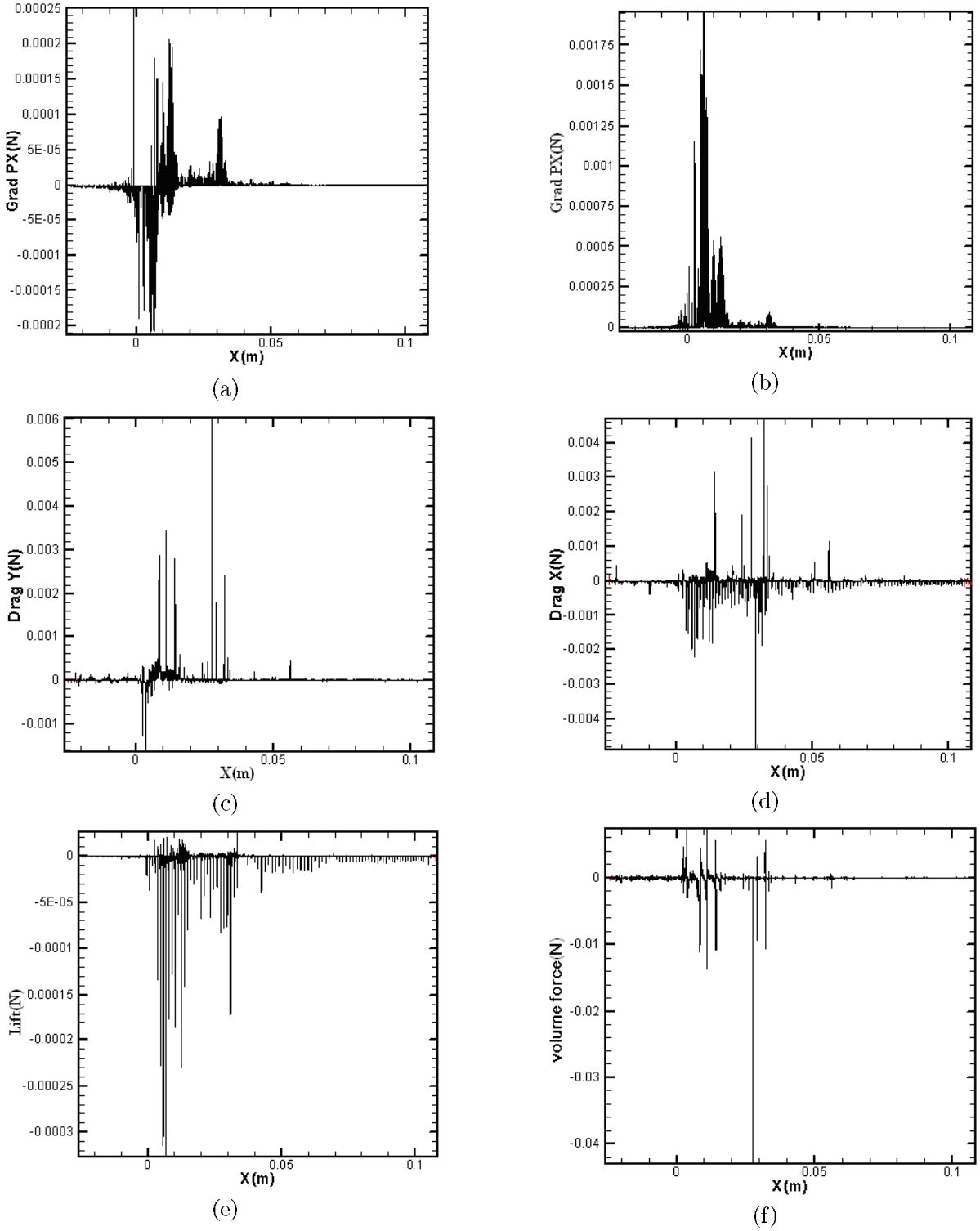

Figure 5. The variation of various forces during the bubble motion for $\mathrm{Re} = 8 \times 10^5, \alpha = 4°$. (a) Pressure gradient force in the X- direction, (b) Pressure gradient force in the Y- direction, (c) Drag force in the Y-direction, (d) Drag force in the X-direction, (e) Saffman lift force and (f) Force due to volume variation.

- The fluctuating velocity components of the fluid have a significant effect on the bubble trajectory.
- Increasing the angle of attack of the hydrofoil will cause a great increase in critical cavitation number

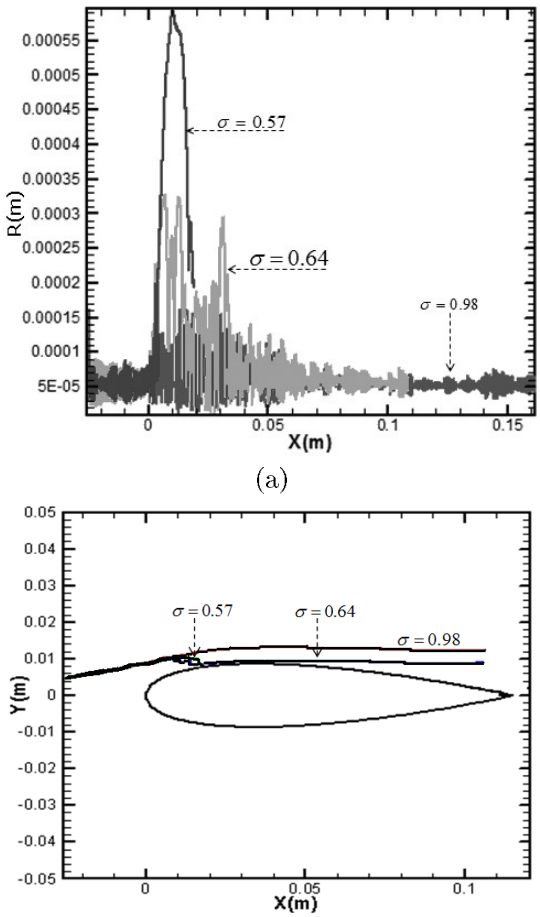

Figure 6. Bubble dynamics for $\mathrm{Re} = 8 \times 10^5, \alpha = 4°$ at different cavitation numbers. (a) Bubble radius and (b) Bubble trajectory.

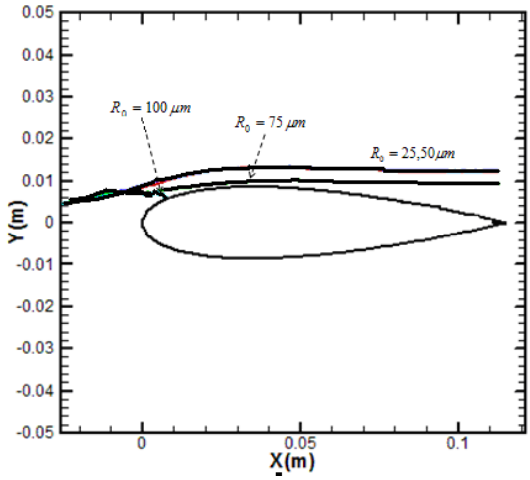

Figure 7. The effect of initial bubble size on its trajectory for $\mathrm{Re} = 8 \times 10^5, \sigma = 0.98, \alpha = 4$.

and consequently the bubble path far away from hydrofoil.

- The bubble initial radius on entering to the domain has a direct effect on its path because of the dependency of hydrodynamic forces on the bubble radius.
- By increasing the cavitation number, the maximum radius of the bubble is decreased.

ACKNOWLEDGEMENT

The authors would like to appreciate the financial support of Research Affairs Department of K.N.Toosi University of Technology.

REFERENCES

1. Lertnuwat, B., Sugiyama, K., "Modeling of Thermal Behavior Inside a Bubble", *CAV2001, Session B6.002*, (2001).
2. Vladislav, A., "Differential Criterion of a Bubble Collapse in Viscous Liquids", *Physical Review E*, **60(1)**, PP 504-509(1999).
3. Hilgenfeldt. S., Brenner. M., "Analysis of Rayliegh - Plesset Dynamics for Sonoluminescins Bubble", *J. Fluid Mechanic*, Department of Mathematic, MIT, Cambridge, (1998).

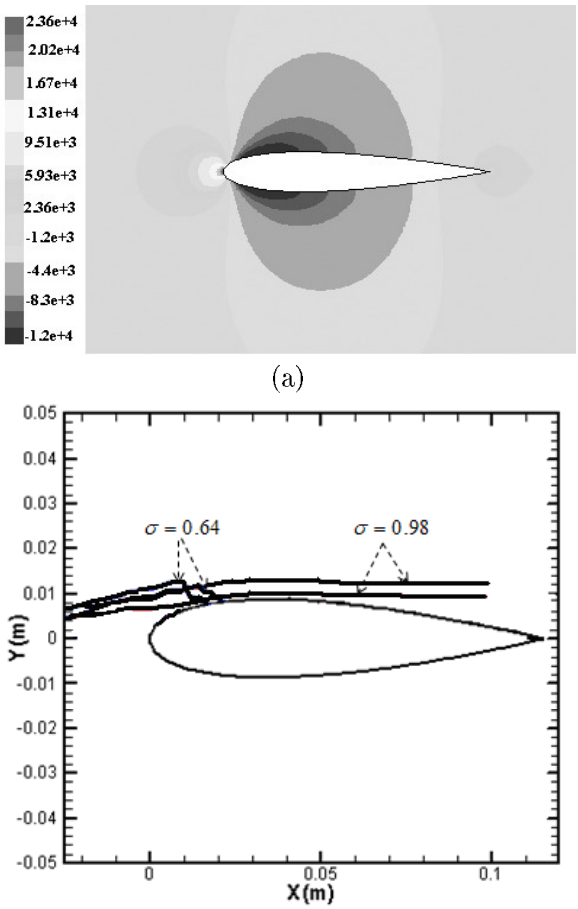

Figure 8. The effect of the angle of attack and cavitation number on the flow and bubble motion for $\mathrm{Re} = 8 \times 10^5, R_0 = 50\mu m, \alpha = 0$. (a) Contour of static pressure and (b) Bubble trajectory.

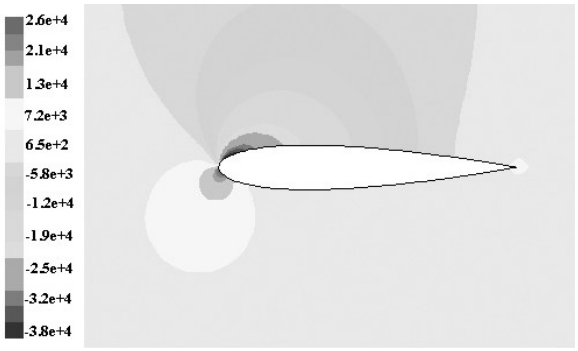

(a)

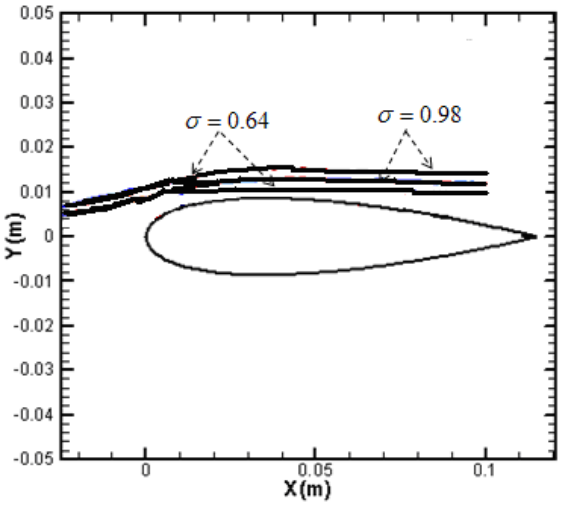

(b)

Figure 9. The effect of the angle of attack and cavitation number on the flow and bubble motion for $\mathrm{Re} = 8 \times 10^5, R_0 = 50\mu m, \alpha = 6$. (a) Contour of static pressure and (b) Bubble trajectory.

4. Brennen, C. E., "Cavitation and Bubble Dynamics", Oxford University, (1995).
5. Meyer, R. S., Billet, M. L., and Holl, J. W., "Numerical Simulation of the Cavitation on a Schiebe Headform", *J. Fluids Eng.*, PP 672-779(1992).
6. Chahine, G. L., "Numerical Simulation of Cavitation Dynamics", *Dynaflow*, inc. 7210 Pindell School Road. Fulton, Maryland 20759, USA., (1997).
7. Farrell, K. J., "Eulerian/Lagrangian analysis for the prediction of cavitation inception", *CAV2001, Session A1.003*, (2001).
8. Delale, C. F., "Steady-State Cavitating Nozzle Flows With Nucleation", *Fifth International Symposium on Cavitation (Cav2003-Cav03-GS-4-001)*, (2003).
9. Zhang, X., Ahmadi, G., "Eulerian-Lagraungian Simulations of Liquid - Gas - Solid Flows in Three - Phase Slurry Reactors", *Chemical Engineering Science*, **60**, PP 5091-5106(2005).
10. Launder, B. F., Reece. G. J., "Progress in The Development of a Reynolds Stress Turbulent Closure", *J. Fluid Mech* , **68**, PP 537-538(1975).
11. Shams, M., Ahmadi, G., "Computational Modeling of Flow and Sediment Transport and Deposition in Meandering Rivers", *Advances in Water Resources*, **25**, PP 689-699(2002).
12. Thomson, D. J., "Criteria for the Selection of Stochastic Models of Particle Trajectories in Turbulent Flows", *J. Fluid Mech.*, **180**, PP 529-556.
13. He, C. H., Ahmadi, G., "Particle Deposition in a Nearly Developed Turbulent Duct Flow with Electrophoresis", *J.Aerosol Sci.*, **30(6)**, PP 739-758(1999).
14. Daly, B. J. and Harlow, F. H., "Transport Equation in Turbulence", *Aerosol Sci. Technol.*, **11**, PP 133-143(1970).
15. Hsiao, C. T., Chain, G., "Scaling Effect on Bubble Dynamics in Tip vortex Flow", *Dynaflow,inc.Report 98007-1*, (2000).
16. Hsiao, C. T., Chorine, G., "Prediction of Vortex Cavitation Inception Using Coupled Spherical and Non - Spherical Models and UnRANS Computations", *Symposium on Naval Hydrodynamics Fukooka*, JAPAN, PP 8-13(2002).
17. Basset, A. B., "A Treatise on Hydrodynamics", Deighton, Bell and Co., Cambridge, England., **12**, (1888).
18. Boussinesq, J., "Theorie Analytique de la Chaleur", Gauthier - Villars, Paris., **12**, PP 224(1903).
19. Maxey, M. R., Riley, J. J., "Equation of Motion for a Small Rigid Sphere in a Nonuniform Flow", *Phys. Fluids*, **26(4)**, PP 883-889(1983).
20. Ahmadi, G., "Introduction to Mechanics of Aerosol With a Review of Recent Computational Methods", Clarkson University, Potsdam. NY., (1996).
21. Shams, M., Ahmadi, G. And Rahimzadeh, H., "Nano Particle Deposition in a Turbulent Duct", *J.Chem.Engn.Sci*, (2000).
22. Haberman, W.L, Morton, R.K., "An Experimental Investigation of the Drag and the Shape of Air Bubble Rising in Various Liquids", *DTMB Report*, (1953).
23. Rapposelli, E., Cervone, A., "Thermal Cavitation Experiments of a NACA 0015 Hydrofoil", 4TH ASME_JSME Joint Fluids Engineering Conference, Honolulu, Hawall, USA, PP 6-11(2003).